Annals of 3D Printed Medicine 18 (2025) 100194

Contents lists available at ScienceDirect

Annals of 3D Printed Medicine

journal homepage: www.elsevier.com/locate/stlm

Research paper

Mechanical characterization of low-cost 3D FDM printed scaffolds fabricated with synthesized PLA/HA bio-composite filament

Mynmayh Khamvongsa [a], Kent Milton [b], Tanvir R. Faisal [b,*]

[a] Dept. of Chemical Engineering, University of Louisiana at Lafayette, LA 70503, USA
[b] Dept. of Mechanical Engineering, University of Louisiana at Lafayette, LA 70503, USA

ARTICLE INFO

Keywords:
Bio-composite
Poly lactic acid (PLA)
Hydroxyapatite (HA)
Bone scaffold
Tissue engineering

ABSTRACT

Bone tissue engineering has gained popularity as a potential alternative in bone defect treatment, where the synthetic graft can be generated by a 3D biomaterial framework (scaffold) that yields shape and initial mechanical strength to facilitate cell bone formation. Biopolymer-based, Poly Lactic Acid (PLA)/Hydroxyapatite (HA) scaffolds were found to have a similar structure, composition, and mechanical properties as natural bone. The objective of this work was to fabricate 3D scaffolds with PLA and HA using a low-cost fabrication process such as Fused Deposition Modeling (FDM), which can be used to construct scaffolds tailored to an individual's specific need in a controlled and customizable process. The study primarily focuses on the synthesis, and mechanical and morphological characterization of PLA/HA filament and its scaffolds. The fabricated 3D printed PLA/HA scaffolds had an interconnected and highly porous structure, resembling natural bone porosity. The addition of HA had a significant effect on the PLA/HA composites although there are no notable differences in mechanical properties between 10–15 % PLA/HA composites. The microstructural morphology of the PLA and PLA/HA composite filaments observed under Scanning Electron Microscopy (SEM) showed a relatively well mixed and homogenous mixture and Energy-dispersive X-ray Spectroscopy (EDS) testing of the filaments' surface topography further showed a mostly homogeneous presence of HA throughout. The 3D printed scaffolds showed a larger pore size due to the inclusion of HA. Additionally, with the increased percentage of HA, the pores became more uneven and irregular. The preliminary results of this study show a promising potential for personalized scaffold design for bone tissue regeneration.

1. Introduction

Bone fractures and segmental bone defects are one of the major causes of patient morbidity, and a source of staggering economic burden worldwide on healthcare systems particularly in orthopedics. In 2019, around 178 million bone fractures occurred globally—a 33.4 % increase since 1990 [1]. Numbers are predicted to increase due to higher incidence of accidents, diseases, and age-related developmental damage [2]. These fractures and defects have a significant negative impact on both the patients' quality of life and society by contributing to economic burdens, including rising healthcare costs, workforce loss, and an increased strain on social services [3]. Bone grafting is the common method to repair bone fractures either by filling in the areas of missing bone with transplanted bone or providing mechanical support to stimulate new bone formation [4]. Each year, nearly 2.2 million bone grafting procedures are done worldwide including autografts (from the patient him/herself), allografts (from a donor), and synthetic grafts [5,6]. However, the availability of suitable bones—both autografts and allografts—are limited. Furthermore, there is an increased risk of infection and possibility of graft rejection as well as donor-site morbidity that can result in chronic pain and discomfort [2,6]. In addition, an autograft or allograft may not be in the correct shape needed to repair the injury. Consequently, synthetic graft became a popular substitute for its easy fabrication, low disease transmission, and relatively low cost.

Bone tissue engineering has gained popularity as a potential alternative in bone defect treatment, where the synthetic graft can be generated by a three-dimensional (3D) biomaterial framework (scaffold) that yields shape and initial mechanical strength to facilitate cell bone formation [7]. Scaffold materials can be synthetic or biologic [8] as well as degradable or nondegradable [9] to facilitate the proliferation, migration, and differentiation of bone cells for bone repair. Polymers have been widely used as biomaterials for the fabrication of

* Corresponding author at: 241 E Lewis St., University of Louisiana at Lafayette, Lafayette, LA 70503, USA.
E-mail address: tanvir.faisal@louisiana.edu (T.R. Faisal).

https://doi.org/10.1016/j.stlm.2025.100194
Received 15 September 2024; Received in revised form 15 December 2024; Accepted 6 February 2025
Available online 7 February 2025

Table 1
Weight compositions of PLA/HA composite filaments.

Type	PLA (wt%)	HA (wt%)
PLA (Control)	100	0
PLA/HA5	95	5
PLA/ HA10	90	10
PLA/HA15	85	15

tissue-engineered scaffolds [10,11]. Polymeric scaffolds [12–15] are being widely used because of their unique properties such as high surface-to-volume ratio, high porosity with smaller pore size, biocompatibility, and engineered mechanical properties. The properties of polymers primarily depend on the composition, structure, and arrangement of their constituent macromolecules. Compared with natural polymers, synthetic polymers are widely used in tissue engineering since their morphology and mechanical properties can be easily tailored for specific applications. Furthermore, synthetic polymeric scaffolds are often cheaper than biological scaffolds and can be produced in large quantities with a long shelf time. Therefore, the goal of this work is to develop low-cost synthetic (composite) biopolymer-based scaffolds for bone tissue engineering.

Bone scaffolds are engineered to closely mimic natural bone to promote tissue growth either *in vitro* or *in vivo*, where the scaffold should have sufficient mechanical properties to support weight or compressive load in addition to biocompatibility and biodegradability [16–18]. Ideally, the scaffold would be custom fitted to the damaged area and structurally stable enough to temporarily take the place of the bone to facilitate the natural growth of the patient's bone. To help stimulate optimal bone growth on the scaffold, a porous structure is required since the available surface area affects cell seeding and penetration [16, 18–23]. Furthermore, scaffolds should be compatible for the bone to grow (osteoconductive) on its surface [24] and capable of inducing multipotent Mesenchymal Stem Cells (MSCs) to the surrounding tissues to differentiate into osteogenic cells to later develop into osteoblasts, bone forming cells [25]. These requirements can be significantly affected by the type of material used in scaffold.

Poly Lactic Acid (PLA) is a synthetic polymer and a good candidate for bone tissue engineering for its biocompatible (mostly bioinertness) and biodegradable [26–29] properties. However, the major limitation of PLA that primarily restricts its use in the fabrication of bone scaffolds include low cell affinity [30,31]. The integration of ceramics surprisingly helps overcome the hydrophobicity of PLA and stimulate the osteoinduction and osteointegration of the implanted scaffold [32]. Considering PLA as a base for a composite, hydroxyapatite (HA, $Ca_5(PO_4)_3(OH)$) is selected as a potential bone-regenerating functionalization agent. HA is a bioactive, nontoxic, osteoinductive, and osteoconductive ceramic mineral commonly used in bone scaffolds due to HA's close analogy to the mineral portion of bones and teeth [33,34],

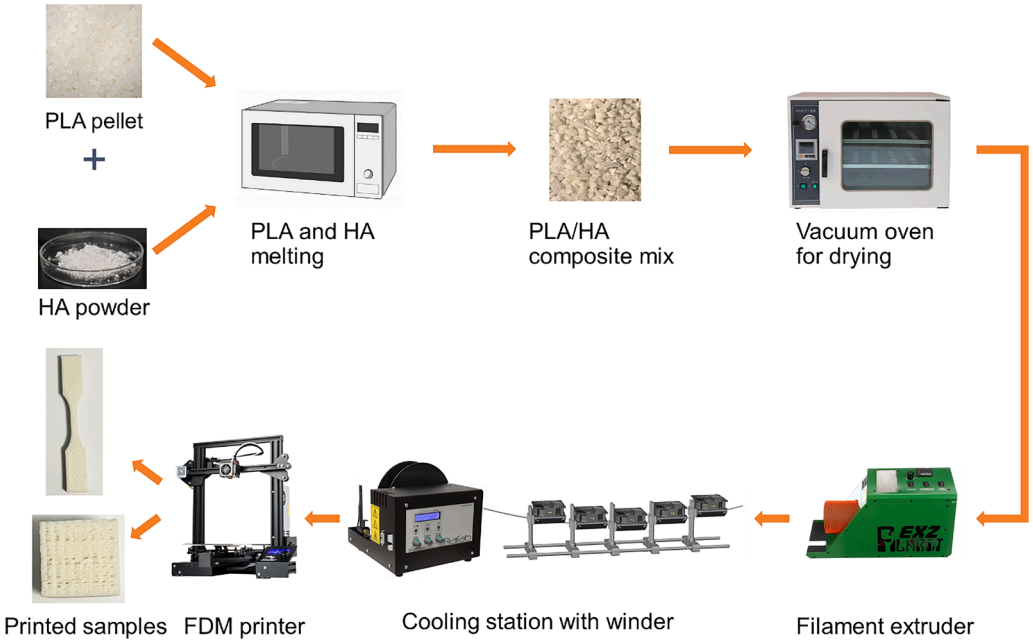

Fig. 1. Overview of workflow from the synthesis of PLA/HA composite filament to the fabrication of 3D printed scaffolds.

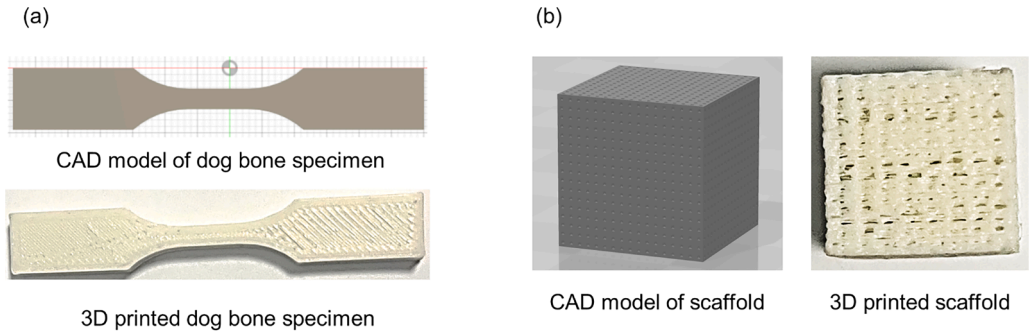

Fig. 2. CAD model and corresponding 3D printed dog-bone specimen (a) and cubic lattice (b).

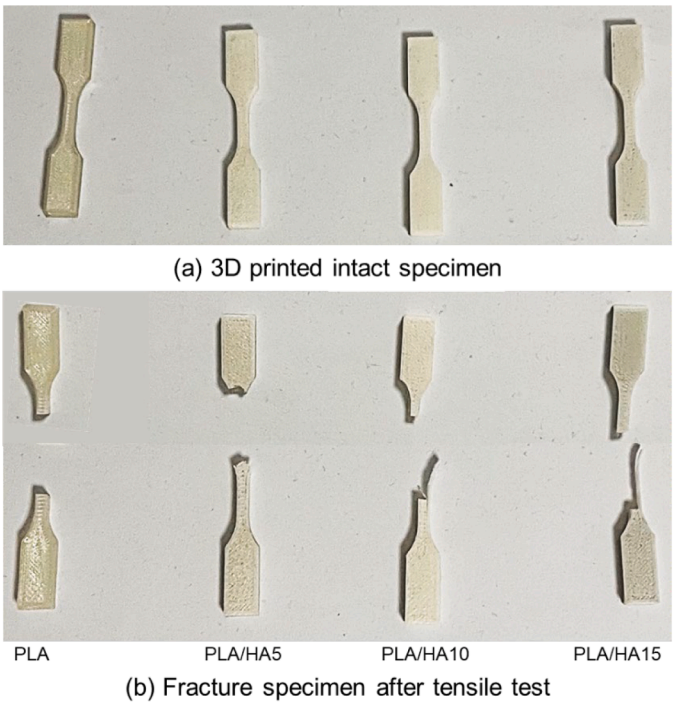

Fig. 3. (a) 3D printed dog bone specimens of PLA and PLA/HA composites, and (b) Fracture patterns of specimens after the tensile test.

and its capacity to form direct chemical bonds with living tissues [35]. In this context, the combination of PLA with HA (PLA/HA) could result in polymer composites with increased level of bioactivity and regeneration potential for bone tissue engineering, overcoming the limitation of individual constituents [16,36–41]. Furthermore, PLA/HA scaffolds were found to have a similar structure, composition, and mechanical properties as natural bone [27].

Even though PLA/HA composites have been widely studied, there are few studies considering the higher weight-percentage of HA ratios [42–44]. The main advantage of adding HA to PLA is to achieve improved osteoconductivity and osteoinduction, which can better facilitate integration with bone tissue [17]. Therefore, using a higher ratio of HA can improve the inferior biological performance of a strictly PLA scaffold, which exhibits poor performance for tissue integration and regeneration. Recent studies show that HA ratios can go up to 20 – 50 % [45], and a variety of fabrication methods with their own benefits and limitations are utilized for printing with higher percentage of HA composites. However, there are very few studies on higher weight percentages utilizing a simple and mechanistic process for scaffold fabrication as demonstrated in this study, reducing the processing time and involvement of any chemical reagents. Our overarching goal is to grow cells on a mechanically stable structure, which can be produced artificially via different process including additive manufacturing. Therefore, in this work, we aim to fabricate 3D scaffolds with optimized biomechanical properties for bone tissue engineering using a low-cost fabrication process such as Fused Deposition Modeling (FDM), which can be used to construct scaffolds tailored to an individual's specific need in a controlled and customizable process [46–48].

Additive manufacturing, or 3D printed technology, [49] was selected for its flexibility, allowing easy adaptation to various designs, materials, and applications. FDM technique can solve some of the limitations in existing scaffold fabrication methods [17]. For example, FDM eliminates the need for solvents, thereby minimizing toxicity risks left by solvent residue and simplifying post-processing. Compared to fabrication techniques such as solvent casting or leaching, FDM's solvent-free approach makes it safer and more environment friendly, while maintaining the material's biocompatibility. FDM also allows for a precise layer-by-layer deposition of PLA/HA composites that can result in a highly controlled pore architecture and size. This precision surpasses the random or inconsistent porosity observed in techniques like solvent casting or freeze-drying. Therefore, we primarily focused on the synthesis and the mechanical and morphological characterization of PLA/HA filament and scaffolds via 3D FDM printer in this work.

2. Materials and methods

2.1. Materials

A biopolymer, PLA pellets (LX175) was purchased from Filabot (Vermont, USA) with the density of 1.24 g/cm^3, mean size of 3.981 ± 0.145 mm and melting temperature of 155 °C. A bio-ceramic, HA powder (289,396) was procured from Sigma-Aldrich (USA). Polymer matrix composite biomaterials were fabricated by mixing PLA and HA with different weight ratios as shown in Table 1.

2.2. Synthesis of the PLA/HA composite filament

The PLA pellets and HA powder were melted together in a microwave oven for four hours at 175 °C. The mixture was stirred after 30 mins of being in the oven and 30 mins before being taken out of the oven to make a well-mixed homogeneous composite. The composite mixture was then cut into pieces of approximately 5–7 mm in length and dried for nearly 7 h in a dry vacuum oven (DZF Vacuum drying oven, Huanghua Xingchen Instrument Co., Ltd, Huanghua, China) at 60 °C. Afterwards, the composite pellets were fed into the Filabot EX2 Extruder (Filabot, Barre, Vermont, USA) to produce composite filament (Fig. 1). The temperature of the extruder was set to 175 °C. The diameter of fabricated filament varied from 1.5 mm to 1.75 mm. A single fan (FilaFab, Somerset, United Kingdom) was turned on near the extruder nozzle for rapid cooling of the filament to prevent deformation before winding.

2.3. 3D printing of the PLA/HA composite structures

Both control and the PLA/HA composite filaments were used to fabricate dog bone specimens according to ASTM D638–14 standard Type V by using a low-cost 3D FDM printer, Creality Ender 3 (Shenzhen Creality 3D Technology Co. Ltd., Shenzhen, China) (Fig. 1). In this work, the tensile test samples were printed in the face down orientation. For PLA (control) and each PLA/HA composites (PLA/HA5, PLA/HA10, and PLA/HA15), five dog-bone samples were printed with an infill density of 100 % in each batch of printing. Throughout the 3D printing process, a print speed of 50 mm/s was maintained and each batch of five samples took about an hour and a half to print.

3D cubic lattice was fabricated according to ASTM D695–15 Standard, as shown in Fig. 2(b). Each CAD model of the 3D cubic lattice was designed in Solidworks 2020 (Dassault Systèmes - SolidWorks Corporation, Massachusetts, USA) with a dimension of 15 mm in each side. Considering the porosity of cortical bone, ranging from 200 μm to 600 μm [50], the scaffolds were designed with a spherical pore of 300 μm in diameter. This pore size was also chosen as a control variable to determine how the scaffolds' properties were affected by the inclusion of naturally occurring mineral—HA that influences the structural strength of bone and bone regeneration as well. All the cubic lattices were printed with 50 % infill density and consequently, the same porosity to provide adequate space for cell growth and proliferation, resembling the porous structure of natural bone [50]. The scaffolds were printed at a print speed of 30 mm/s with a layer height of 0.2 mm to gain a better quality, which was optimized after several trial prints. Each sample took approximately one hour and a half to print.

The remaining 3D printing settings were optimized specifically for PLA filament to ensure high-quality and well-finished printed samples. All samples were printed using a heated bed temperature of 50 °C and a

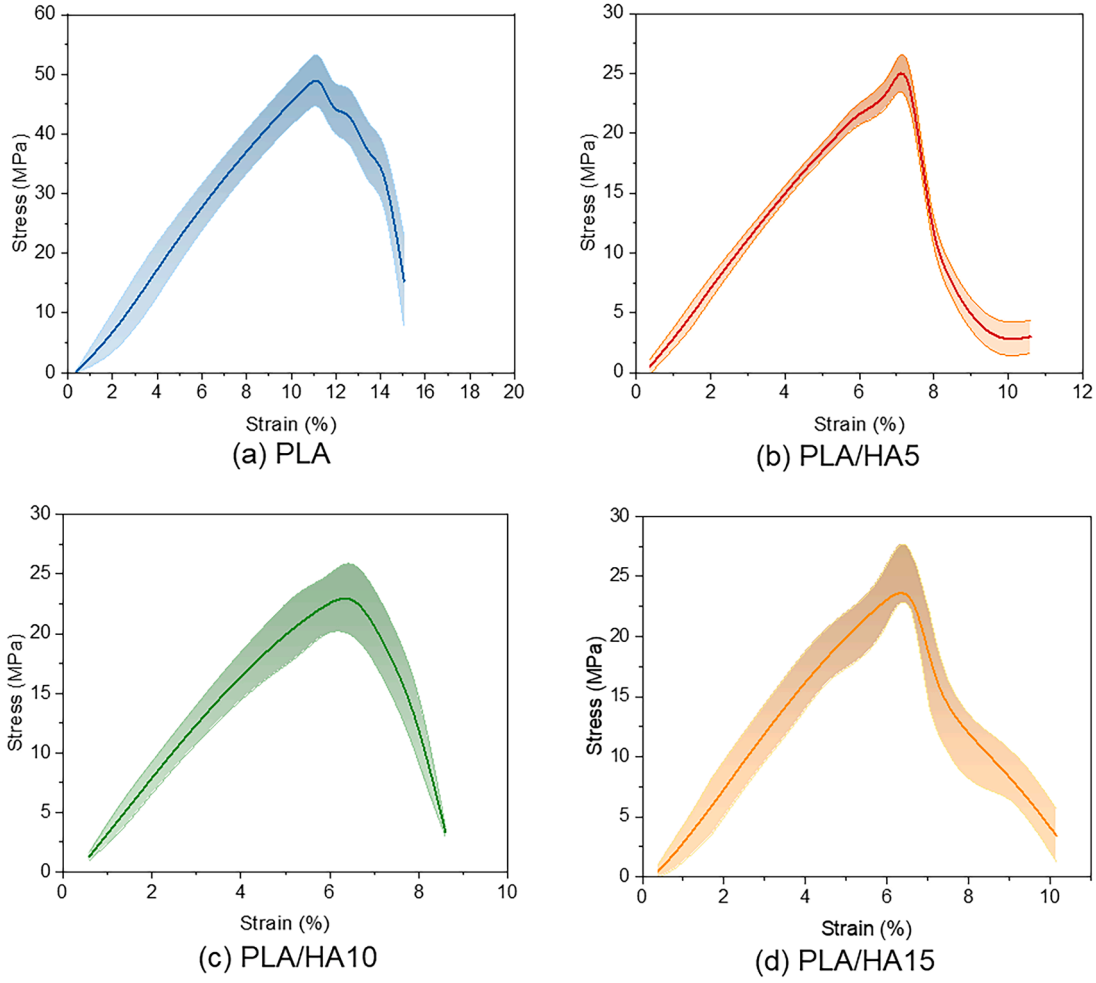

Fig. 4. Stress-strain plot of PLA and PLA/HA composite dog bone specimens under tensile loading.

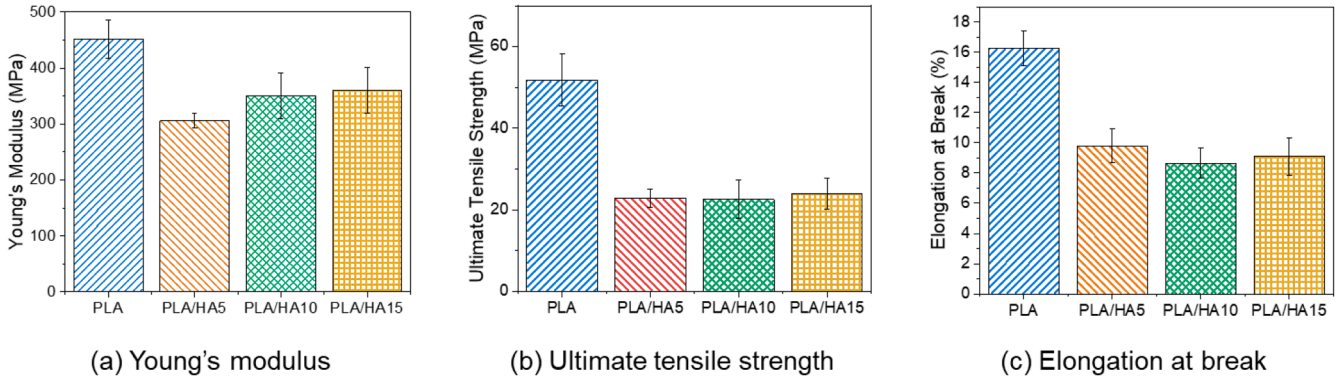

Fig. 5. Mechanical properties of PLA and PLA/HA composites obtained via tensile tests (a) Young's modulus, (b) Modulus of toughness, and (c) Elongation at break.

nozzle temperature of 200 °C. The initial layer speed was 20 mm/s, retraction speed was 45 mm/s, and travel speed was 150 mm/s. Layer height was set to 0.2 mm. The printing parameters were usually chosen based on several factors such as type of filament materials, print quality, nozzle diameter as well as filament diameter, and infill density and pattern. While some printing parameters were chosen as per the standard operating procedure, some were optimized via trial printing and subsequent print quality analysis.

2.4. Scanning electron microscopy (SEM)

SEM micrographs from different filaments and 3D printed scaffolds were used to assess microstructure, pore size, and morphological details of PLA/HA composite structures. Having been coated with 10 nm layer of gold, the SEM micrographs were gathered by the Scios 2 DualBeam (Thermo Fisher Scientific, Massachusetts, USA) SEM system. For the filaments, SEM images were acquired to see how evenly the HA was distributed in PLA, and if there was a significant contrast between the two that results in obvious phases being seen in the cross section. The

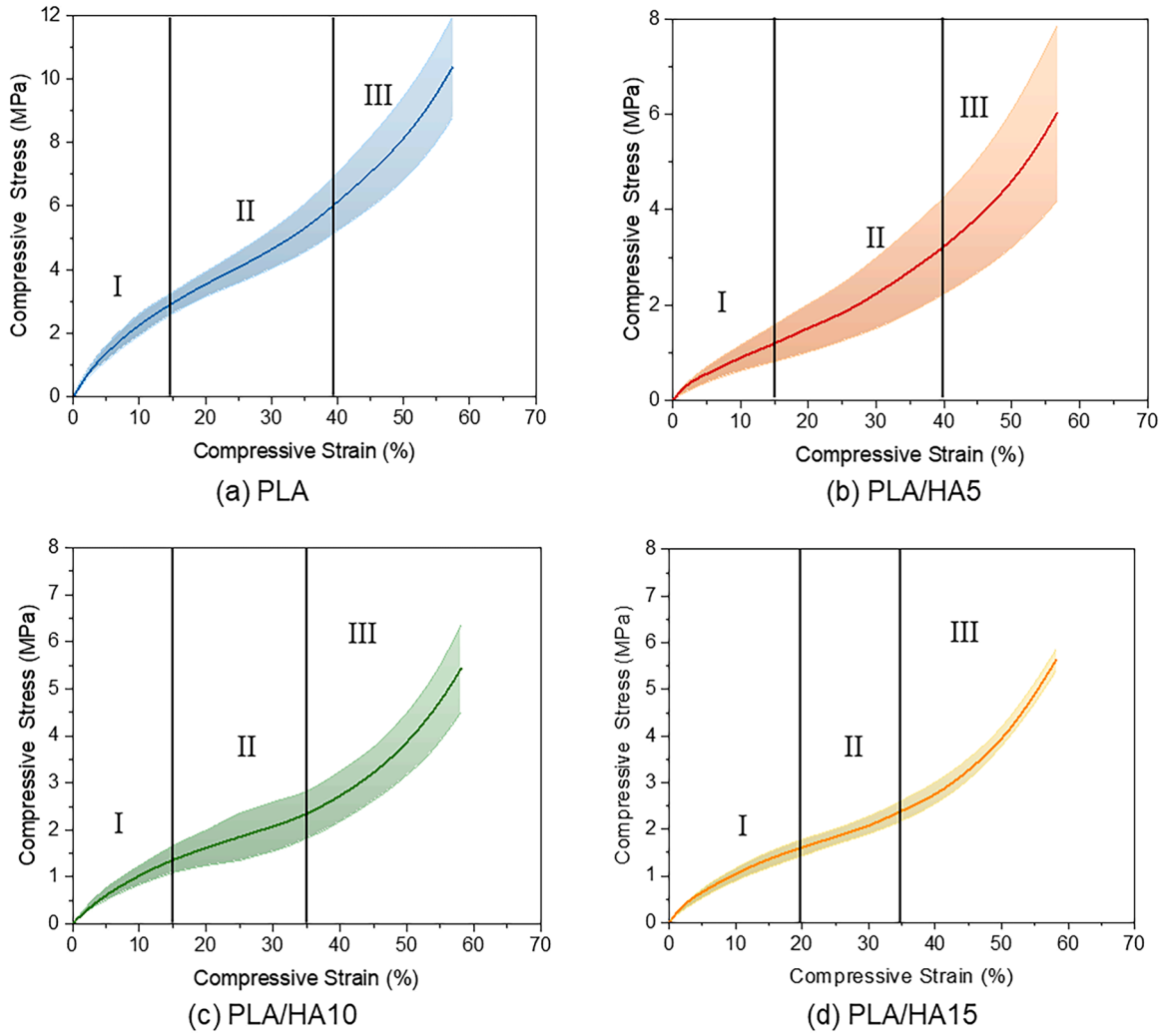

FIG. 6. Stress-strain plot of 3D printed scaffolds under uniaxial compression. I: Linear elastic zone, II: Plateau zone, and III: Densification zone.

SEM was operated using the T1 detector, a backscatter detector, to take images and the voltage was set at 10kV. At each ratio, three samples taken at different sections of the filament were observed, and images were taken at 80x and 10,000x magnification. SEM images of cubic scaffolds were also taken to assess the porous architecture of the structure. The SEM was operated using the Everhart Thornley Detector in secondary electron mode. For each PLA/HA ratio, one sample was observed, and top view and side view images were taken at 200x, 31x, and 27x magnification.

2.5. Energy dispersive X-ray spectroscopy (EDS)

When HA is dispersed very well and is present at nanoscale on a surface, the elemental compositions cannot be differentiated through SEM only. For this, we performed energy dispersive X-ray spectroscopy (EDS) to verify the presence of HA particles in these composites scaffolds' surface as well as to conduct elemental analyses. EDS was performed using a ThermoFisher Scientific Ultradry detector inside a ThermoFisher Scientific Scios 2 microscope operating at 20 kV and analyzed using ThermoFisher Scientific Pathfinder software. In EDS analysis, X-rays from the elements are generated which can be mapped to verify the presence of specific elements. Here, in HA-containing composite scaffolds, X-rays generated from calcium (Ca) and phosphorus (P) were detected and EDS mapping was performed.

2.6. Tensile and compression tests

To evaluate the mechanical properties of the composite filaments and scaffolds, tensile and compression tests were performed with the dog-bone specimen and cubic lattice, respectively, using the 240 Family Electromechanical Universal Test Machine (UTM) (TestResources, Minnesota, USA) with 5 kN load cell. A tensile stress-strain diagram was plotted for each type of tensile specimen to determine the elastic modulus, E (the slope of the stress-strain curve in the elastic region). Tensile test was performed at a speed of 12.7 mm/min (0.5 in/min). Compression test was performed on the cubic scaffolds at a speed of 1.27 mm/min (0.05 in/min). Similarly, a compressive stress-strain diagram was plotted for each type of cubic scaffold to determine its' stiffness, E. Test results were compared at 50 % compression strain.

2.7. Porosity estimation

The porosity of each scaffold was calculated by dividing the mass of the scaffold by what it would have been if the scaffold was made from the same material and solid. The average values of each composition were calculated, and the percentage difference between the average values of height, width, and volume of the printed scaffolds and the height, width, and volume of the 3D scaffold model were taken.

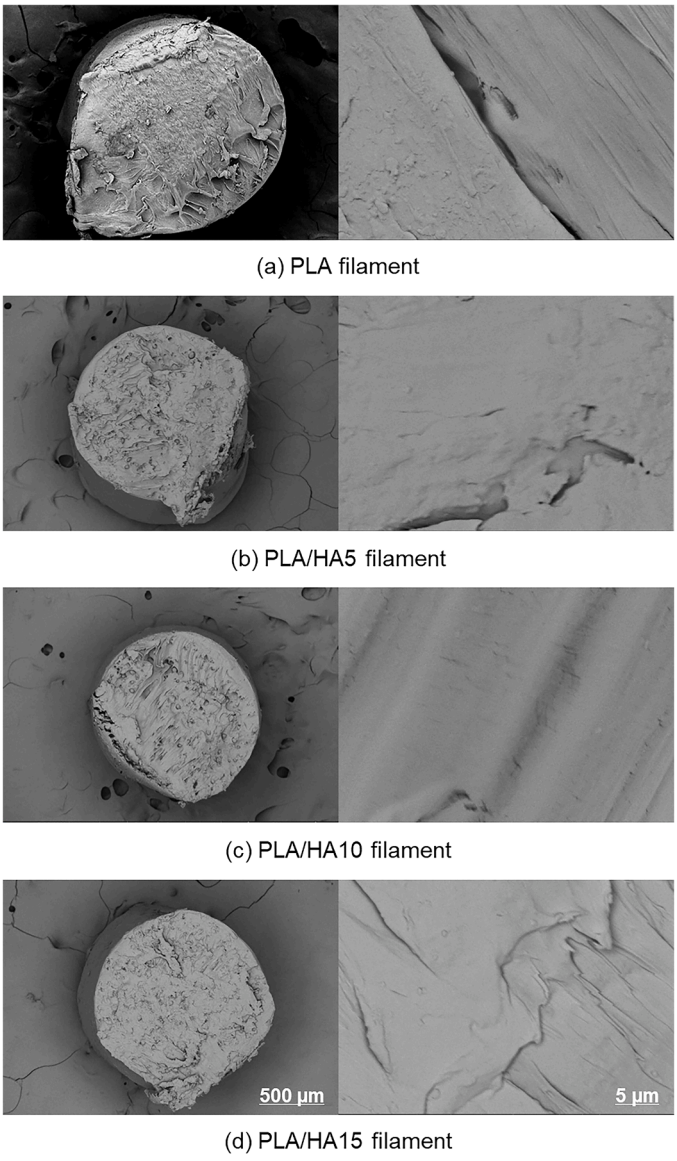

Fig. 7. SEM images taken at 80x (left) and 10,000x (right) magnification of (a) PLA, (b) PLA/HA5, (c) PLA/HA10, and (d) PLA/HA15 filament cross section.

3. Results and discussion

3.1. Tensile test

Mechanical properties of the PLA and PLA/HA composite filaments were evaluated by conducting tensile test of 3D printed dogbone specimen. Each specimen was tested until the complete fracture observed and five specimens were tested for each group. Fig. 3 shows the intact 3D printed dogbone specimens of PLA (control) and PLA/HA5, PLA/HA10, and PLA/HA15 composites (Fig. 3a), and the corresponding specimens after the complete fracture (Fig. 3b). During tensile testing, fracture was observed and it was determined that the specimens' fracture characteristics depend on the amount of HA present in them. As we can see, the control specimens (PLA only) exhibited straight breaks when pulled apart during testing, resembling ductile fracture. PLA/HA5 experienced jaggedness focused on the break area. PLA/HA10 and PLA/HA15 performed similarly, exhibiting similar mechanical properties. They both have more of a jagged breakdown in the middle where it split in the side, and the jaggedness is more pronounced than the other two groups. The addition of HA in the specimens showed a correlation with the specimens having more jagged breaks, indicating a brittle fracture.

Fig. 4 displays the tensile stress versus tensile strain behavior for the control (PLA only) and the PLA/HA composite specimens. It is evident that tensile strength of PLA specimen (Fig. 4a) is significantly higher than PLA/HA composites (Fig. 4b–4d). In addition, with increasing percentage of HA, the elongation at break decreases for PLA/HA composites.

The stress-strain plots show that the tensile yield strain and yield stress are significantly decreased as HA is added. The PLA specimens can handle more than double the maximum (yield) stress load than the specimens containing HA. A notable decrease in yield strain and stress is observed as the amount of HA in the PLA/HA composite increases. However, we see that the variations of yield stress and stain are minimal between PLA/HA10 and PLA/HA15. The addition of HA lowered the Young's modulus, but as the amount of HA increased in the specimens, the stiffness increased as well (Fig. 5a). Both modulus of toughness and elongation at break (Fig. 5b–5c) also reduced in the PLA/HA composites in comparison with control (PLA only) specimen.

The higher the percentage of elongation at break and the modulus of toughness, the more ductile a material is. For both elongation at break and modulus of toughness, the control group had significantly higher values than the specimens containing HA. The addition of HA correlates with a decrease in modulus of toughness and an increase in brittleness, which aligns with the characteristics of ceramic minerals. The incorporation of more minerals in a composite tends to result in increased brittleness. PLA, a thermoplastic material, combind with more minerals, exhibits decreased ductility. However, there is no observable pattern or trend that links the increased amounts of HA in the specimens to changes in ductility.

3.2. Compression test

Compression tests were performed on 15 mm cube scaffolds with ~60 % of strain, and the resulting stress strain curves are shown in Fig. 6. All the specimens bulged during testing irrespective of the compositions. As we can see, the scaffolds made of only PLA filament can withstand more compressive stress than the PLA/HA composites for nearly same amount of deformation. Adding HA reduces the compressive load bearing capacity of the scaffolds, with minimal difference observed between PLA/HA10 and PLA/HA15. However, it is anticipated that the linear elastic zone (I) is slightly increased in PLA/HA15 scaffolds. More importantly, the plateau zone (II) gradually decreases as the percentage of HA increases, indicating reduction of energy absorption capacity of the scaffolds. Additionally, the densification started slightly earlier in PLA/HA10 and PLA/HA15. It is apparent that the scaffolds with PLA/HA composites have less comprehensive strength than PLA only scaffolds.

3.3. Morphological characterization

The microstructural morphology of the PLA and PLA/HA composites filaments was observed under SEM. The surface topography and the distribution of HA in the filaments' cross sections are shown in SEM micrographs obtained with 80x and 10,000x magnifications (Fig. 7). The high-resolution images show the PLA and HA are relatively well mixed and homogenous. The discrepancies (dark spots, bumpiness, etc.) in each filament's surface can be attributed to the method of sample collections from the filament. Normally, a sample is cut using a razor blade, but we used a scissor instead, because the filaments were small and thin.

The morphology of the 3D printed porous scaffolds was also evaluated under SEM with 200x magnification (Fig. 8). The surface topography of the cross sections shows the presence of a bumpy surface across all ratios, more evident in the samples that contain HA. However, since it is also present in control samples, the surface texture can possibly be attributed to the PLA not being fully melted, an additive manufacturing issue with the 3D printer being at fault, or the presence of too much

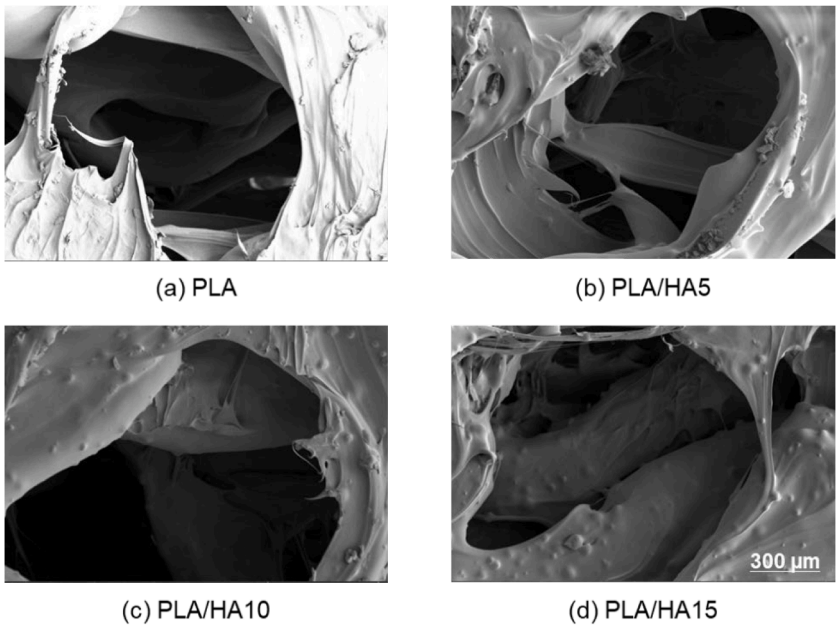

Fig. 8. SEM images taken at 200x magnification of cubic scaffolds 3D printed with (a) PLA, (b) PLA/HA5, (iii) PLA/HA10, and (d) PLA/HA15 filaments.

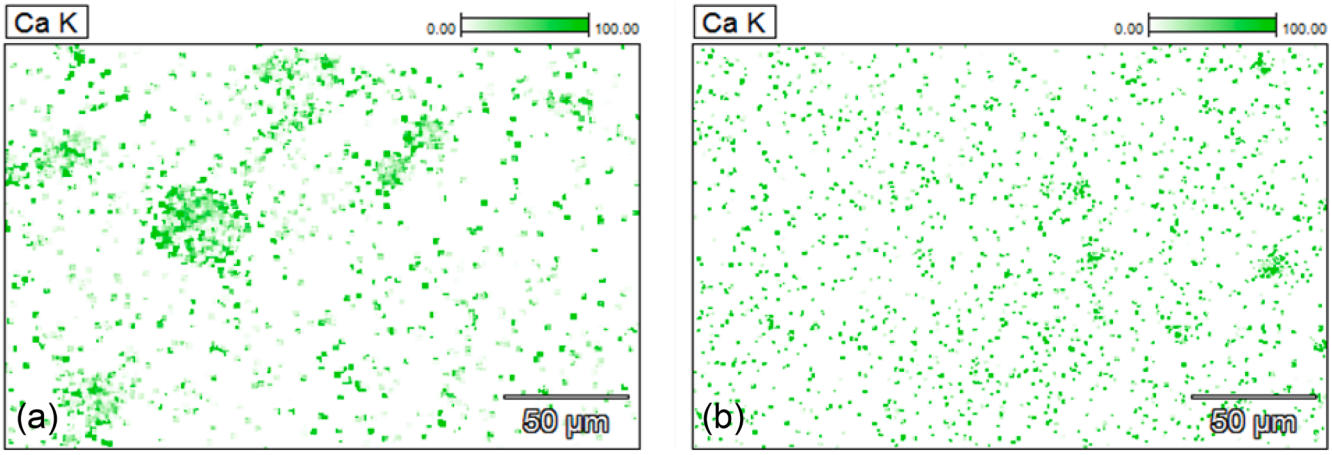

Fig. 9. EDS results of unevenly (left) and evenly (right) distributed calcium phosphate.

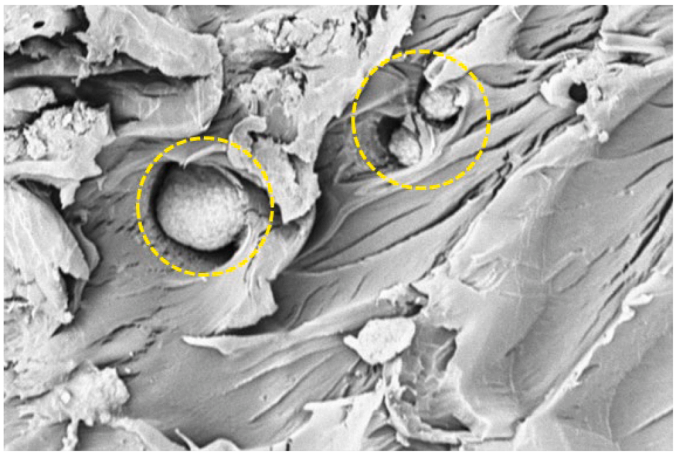

Fig. 10. Spherical objects (unmixed calcium phosphate, circled) embedded in PLA/HA composites observed in SEM images at 800x magnifications.

Table 2
Average percent difference (mean ±SD) between 3D printed scaffold and CAD model.

Scaffold Type	Δ_{Height} (%)	Δ_{Width} (%)	Δ_{Volume} (%)
PLA	0.43 ± 0.283	3.08 ± 0.609	6.10 ± 1.246
PLA/HA5	0.16 ± 0.088	2.41 ± 0.318	4.75 ± 0.713
PLA/HA510	0.25 ± 0.097	2.77 ± 0.466	5.43 ± 1.118
PLA/HA15	0.27 ± 0.028	3.12 ± 0.72	6.30 ± 1.737

Table 3
Porosity of PLA and PLA/HA composite scaffolds.

Scaffold Type	PLA	PLA/HA5	PLA/HA10	PLA/HA15
Porosity (%)	57.99	75.73	74.39	75.34

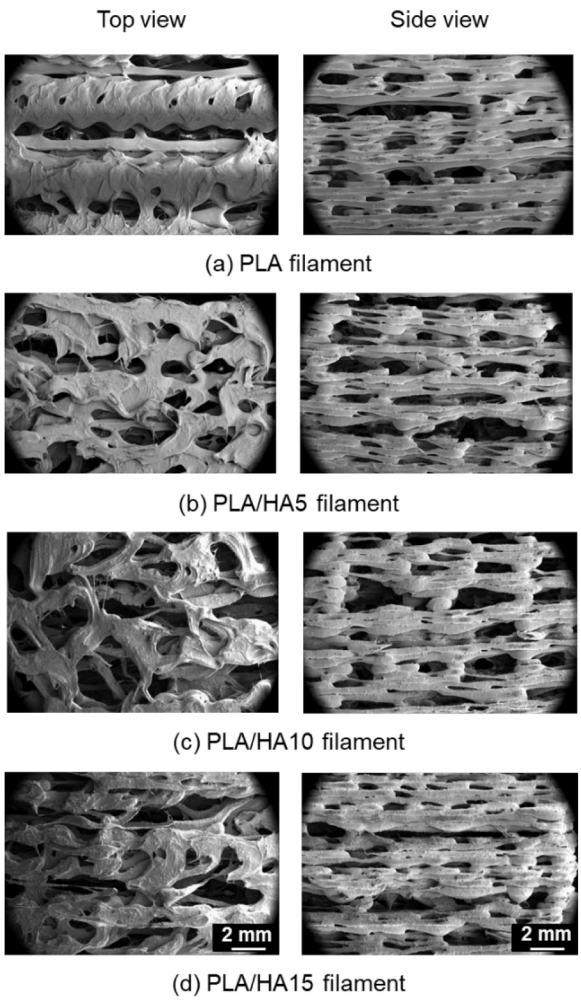

Fig. 11. SEM images taken at 31x (left) of the top view and 27x (right) magnification of the side view of cubic scaffolds printed with (a) PLA, (b) PLA/HA5, (c) PLA/HA10, and (d) PLA/HA15 filament.

moisture before printing.

3.4. Elemental analysis

The EDS test was done to find out the distribution of elements on the filament's surface. The EDS showed mostly a homogeneous presence of HA throughout. All the samples of PLA/HA5 were evenly distributed and read as one solid material by the equipment with no distinct phases that can be seen. For PLA/HA10 and PLA/HA15, three samples out of five were similarly read as a homogenous distribution. The constituents in the filaments may not have been well mixed, especially when the amount of HA increases, and therefore distinct HA and PLA phases can be seen. Fig. 9 depicts the difference in EDS results between unevenly (Fig. 19a) and evenly (Fig. 9b) distributed mixtures. When HA is unevenly distributed, it tends to agglomerate, contrasting with samples where the mixture is more evenly dispersed. The presence of distinct phases helps in distinguishing between even and uneven HA distribution. However, no significant change in the HA percentage is noticaable across the different ratios.

This uneven distribution was also observed in SEM images. Overall, only two of the 15 samples (one in PLA/HA10 and one in PLA/HA15) had small spherical objects embedded (Fig. 10), indicating not evenly amalgamated during melting and filament extrusion process.

3.5. Print quality analysis

The printability of the 3D printed scaffolds was evaluated by comparing the geometry of the CAD model and fabricated scaffolds. Table 2 shows the percentage difference between the average values of height, width, and volume of the printed scaffolds and the 3D CAD models. As observed, all the printed scaffolds on average were scaled up by a factor of 0.0564 in comparison with the CAD model with no clear trend of the amount of HA affecting the scale factor. It is our anticipation that since the components are homogeneously mixed in the extruded filaments, the printability is not much affected by the inclusion of HA particles.

The porosity of the scaffold was designed to be 25 % and printed at a 50 % infill, which increased the porosity. Table 3 shows the porosities of the PLA and PLA/HA composite scaffolds. The porosity increases significantly in all the three PLA/HA composites in comparison with scaffolds printed with PLA only. The scaffold with HA exhibited higher porosity than those without which could have caused the control group to have such a higher compressive strength. However, there is no trend between an increase in volume distortion and HA being added. Also, there is no trend between an increase in HA and porosity aside from the presence of HA creating greater porosity.

The print quality of the 3D printed scaffolds varies based on PLA/HA compositions as observed in Fig. 11. The scaffold printed with only PLA displays relatively consistent and smooth layers with minimal structural irregularities, whereas scaffolds printed with PLA/HA compositions appear rougher and less uniform, resulting in a reduced print quality when compared to the PLA scaffold. As the percentage of HA increases, the pore size increases and the distribution becomes less uniform, suggesting that the higher HA content affects the material's flow characteristics during printing. In addition, the layers of the PLA specimens adhere well to each other with minimal gaps or voids, while the layers of the PLA/HA specimens have gaps that become more prominent with increasing percentage of HA, suggesting a reduced bonding quality, which explains the reduction in mechanical strength of PLA/HA specimens. Overall, the PLA specimens altered withHA show the challenges of maintaining structural integrity as material composition changes.

Since in this work we synthesized biocomposite, the composite's structural integrity and mechanical behavior under various conditions were the prime concern before considering its biological applications. In this study, we only considered the mechanical performance of the 3D printed PLA/HA scaffolds without optimizing the balance between structural properties. The future work will consider design optimization integrating mechanical testing into the design loop. Furthermore, in 3D-printed biomaterials or scaffolds, mechanical properties are often tested to evaluate the feasibility of the fabrication process and assess the structural integrity of the scaffolding materials [51,52]. This ensures consistent and reliable manufacturing before delving into biological performance. However, the limitation of this study is primarily the lack of biological and biodegradation testing, which is necessary to assess the suitability of the fabricated biomaterials for tissue engineering. Therefore, future studies will evaluate biocompatibility, biodegradability, and viability and efficiency of cell growth on 3D-printed scaffolds using the synthesized PLA/HA filament.

We have identified some processing limitations that may affect the mechanical performance of synthesized composite filament and the 3D printed scaffolds. First, for good quality filament extrusion, the PLA pellets must be dried in the oven for a few hours before being used to have as little moisture as possible; otherwise, the extruder cannot extrude a good quality filament. Although the pellets were vacuum dried for hours, moisture may have accumulated during the extrusion process, which is comparatively a slow, gradual process. Second, the addition of HA powder being combined with the PLA pellets results in a filament diameter smaller than the standard 1.75 mm that the 3D printer's nozzle prints with. The resulting filament diameter is on average 1.5 mm. A 1.75 mm nozzle on the 3D printer does have the capability to print at a

smaller diameter, minimum 1.3 mm filament. An alternative method of combining HA powder and PLA pellets before putting the mixture through the extruder or alternative equipment can result in a larger diameter to make it easier for 3D printing specimens in a consistent manner. In addition, it was increasingly difficult to mix HA into PLA as the weight percentage of HA increased and ensured a well-mixed mixture before putting it through the extruder.

4. Conclusions

The goal of this work was to fabricate biopolymer-based 3D scaffolds using PLA and HA with optimized biomechanical properties for bone tissue engineering via FDM, focusing on the impact of higher weight percentages of HA on mechanical and morphological properties. The addition of HA had a significant effect on the PLA/HA composites but increasing the percentage of HA beyond 10–15 % had no notable differences in mechanical properties. Despite the difficulty of mixing the HA into PLA, a homogenous mixture was obtained except for two of the fifteen total samples. It is anticipated from this study that a well-mixed PLA/HA composites can be synthesized using the filament extruder, and the extruded filaments can be used for 3D printed scaffolds with pore size similar to cortical bone. All the scaffolds printed with PLA filament and PLA/HA composite filaments show an interconnected highly porous structure, resembling natural bone [50]. Although this work primarily focused on biomechanical properties of 3D printed scaffolds that exhibit promising result for bone tissue engineering, biological testing will be required to evaluate its complete functionality in tissue regeneration.

Declaration of competing interest

The authors declare the following financial interests/personal relationships which may be considered as potential competing interests:

Tanvir Faisal reports financial support was provided by Louisiana State University. If there are other authors, they declare that they have no known competing financial interests or personal relationships that could have appeared to influence the work reported in this paper.

Acknowledgment

The authors gratefully acknowledge the financial support from Louisiana Materials Design Alliance (LEQSF-EPS(2022)-LAMDASeed-Track1A-09). The authors also acknowledge the technical support from Lily Hume of UL Lafayette Microscopy Center in acquiring SEM images

References

[1] Wu, A.-M., Bisignano, C., James, S.L., Abady, G.G., Abedi, A., Abu-Gharbieh, E., Alhassan, R.K., Alipour, V., Arabloo, J., Asaad, M., Asmare, W. N., Awedew, A. F., Banach, M., Banerjee, S. K., Bijani, A., Birhanu, T. T. M., Bolla, S. R., Cámera, L. A., Chang, J.-C., Cho, D. Y., Chung, M. T., Couto, R. A. S., Dai, X., Dandona, L., Dandona, R., Farzadfar, F., Filip, I., Fischer, F., Fomenkov, A. A., Gill, T. K., Gupta, B., Haagsma, J. A., Haj-Mirzaian, A., Hamidi, S., Hay, S. I., Ilic, I. M., Ilic, M. D., Ivers, R. Q., Jürisson, M., Kalhor, R., Kanchan, T., Kavetskyy, T., Khalilov, R., Khan, E. A., Khan, M., Kneib, C. J., Krishnamoorthy, V., Kumar, G. A., Kumar, N., Lalloo, R., Lasrado, S., Lim, S. S., Liu, Z., Manafi, A., Manafi, N., Menezes, R. G., Meretoja, T. J., Miazgowski, B., Miller, T. R., Mohammad, Y., Mohammadian-Hafshejani, A., Mokdad, A. H., Murray, C. J. L., Naderi, M., Naimzada, M. D., Nayak, V. C., Nguyen, C. T., Nikbakhsh, R., Olagunju, A. T., Otstavnov, N., Otstavnov, S. S., Padubidri, J. R., Pereira, J., Pham, H. Q., Pinheiro, M., Polinder, S., Pourchamani, H., Rabiee, N., Radfar, A., Rahman, M. H. U., Rawaf, D. L., Rawaf, S., Saeb, M. R., Samy, A. M., Sanchez Riera, L., Schwebel, D. C., Shahabi, S., Shaikh, M. A., Soheili, A., Tabarés-Seisdedos, R., Tovani-Palone, M. R., Tran, B. X., Travillian, R. S., Valdez, P. R., Vasankari, T. J., Velazquez, D. Z., Venketasubramanian, N., Vu, G. T., Zhang, Z.-J., and Vos, T., 2021, "Global, regional, and national burden of bone fractures in 204 countries and territories, 1990–2019: a systematic analysis from the Global Burden of Disease Study 2019," Lancet Healthy Long., 2(9), pp. e580–92.

[2] Bisht B, Hope A, Mukherjee A, Paul MK. Advances in the fabrication of scaffold and 3D printing of biomimetic bone graft. Ann Biomed Eng 2021;49(4):1128–50.

[3] Alonso-Fernández I, Haugen HJ, López-Peña M, González-Cantalapiedra A, Muñoz F. Use of 3D-printed polylactic acid/bioceramic composite scaffolds for bone tissue engineering in preclinical in vivo studies: a systematic review. Acta Biomater 2023;168:1–21.

[4] Zhao R, Yang R, Cooper PR, Khurshid Z, Shavandi A, Ratnayake J. Bone grafts and substitutes in dentistry: a review of current trends and developments. Molecules 2021;26(10):3007.

[5] Archunan MW, Petronis S. Bone grafts in trauma and orthopaedics. Cureus 2021;13(9):e17705.

[6] Lewandrowski K-U, Gresser JD, Wise DL, Trantolo DJ. Bioresorbable bone graft substitutes of different osteoconductivities: a histologic evaluation of osteointegration of poly (propylene glycol-co-fumaric acid)-based cement implants in rats. Biomaterials 2000;21(8):757–64.

[7] Ghassemi T, Shahroodi A, Ebrahimzadeh MH, Mousavian A, Movaffagh J, Moradi A. Current concepts in scaffolding for bone tissue engineering. Arch Bone Jt Surg 2018;6(2):90.

[8] Qu H, Fu H, Han Z, Sun Y. Biomaterials for bone tissue engineering scaffolds: a review. RSC Adv 2019;9(45):26252–62.

[9] Reddy MSB, Ponnamma D, Choudhary R, Sadasivuni KK. A comparative review of natural and synthetic biopolymer composite scaffolds. Polymers (Basel) 2021;13(7).

[10] Piskin E. Biodegradable polymers as biomaterials. J. Biomater. Sci. Poly. Edition 1995;6(9):775–95.

[11] Ji Y, Ghosh K, Shu XZ, Li B, Sokolov JC, Prestwich GD, Clark RA, Rafailovich MH. Electrospun three-dimensional hyaluronic acid nanofibrous scaffolds. Biomaterials 2006;27(20):3782–92.

[12] Eaglstein WH, Falanga V. Tissue engineering and the development of Apligraf®, a human skin equivalent. Clin Ther 1997;19(5):894–905.

[13] Boyan BD, Lohmann CH, Romero J, Schwartz Z. Bone and cartilage tissue engineering. Clin Plast Surg 1999;26(4):629–45.

[14] Mayer J, Karamuk E, Akaike T, Wintermantel E. Matrices for tissue engineering-scaffold structure for a bioartificial liver support system. J. controlled release 2000;64(1–3):81–90.

[15] Mayer J, Shin'oka T, Shum-Tim D. Tissue engineering of cardiovascular structures. Curr. Opin. Cardiol. 1997;12:528–32.

[16] Ghassemi T, Shahroodi A, Ebrahimzadeh MH, Mousavian A, Movaffagh J, Moradi A. Current concepts in scaffolding for bone tissue engineering. Arch Bone Jt Surg 2018;6(2):90–9.

[17] Bernardo MP, da Silva BC, Hamouda AE, de Toledo MA, Schalla C, Rütten S, Goetzke R, Mattoso LH, Zenke M, Sechi A. PLA/hydroxyapatite scaffolds exhibit in vitro immunological inertness and promote robust osteogenic differentiation of human mesenchymal stem cells without osteogenic stimuli. Sci Rep 2022;12(1):2333.

[18] Hutmacher DW. Scaffolds in tissue engineering bone and cartilage. Biomaterials 2000;21(24):2529–43.

[19] Porter JR, Ruckh TT, Popat KC. Bone tissue engineering: a review in bone biomimetics and drug delivery strategies. Biotechnol. Prog. 2009;25(6):1539–60.

[20] Lutzweiler G, Ndreu Halili A, Engin Vrana N. The overview of porous, bioactive scaffolds as instructive biomaterials for tissue regeneration and their clinical translation. Pharmaceutics 2020;12(7):602.

[21] Mo X, Xu C, Kotaki M, Ramakrishna S. Electrospun P (LLA-CL) nanofiber: a biomimetic extracellular matrix for smooth muscle cell and endothelial cell proliferation. Biomaterials 2004;25(10):1883–90.

[22] Woodard JR, Hilldore AJ, Lan SK, Park C, Morgan AW, Eurell JAC, Clark SG, Wheeler MB, Jamison RD, Johnson AJW. The mechanical properties and osteoconductivity of hydroxyapatite bone scaffolds with multi-scale porosity. Biomaterials 2007;28(1):45–54.

[23] Hing K, Annaz B, Saeed S, Revell P, Buckland T. Microporosity enhances bioactivity of synthetic bone graft substitutes. J. Mater. Sci.: Mater. Med. 2005;16:467–75.

[24] Albrektsson T, Johansson C. Osteoinduction, osteoconduction and osseointegration. European spine journal 2001;10(Suppl 2):S96–101.

[25] Oryan A, Alidadi S, Moshiri A, Maffulli N. Bone regenerative medicine: classic options, novel strategies, and future directions. J Orthop Surg Res 2014;9(1):1–27.

[26] Hu J, Sun X, Ma H, Xie C, Chen YE, Ma PX. Porous nanofibrous PLLA scaffolds for vascular tissue engineering. Biomaterials 2010;31(31):7971–7.

[27] Zhang B, Wang L, Song P, Pei X, Sun H, Wu L, Zhou C, Wang K, Fan Y, Zhang X. 3D printed bone tissue regenerative PLA/HA scaffolds with comprehensive performance optimizations. Mater Des 2021;201:109490.

[28] Revati R, Majid MA, Ridzuan M, Basaruddin K, Cheng E, Gibson A. In vitro degradation of a 3D porous pennisetum purpureum/PLA biocomposite scaffold. J Mech Behav Biomed Mater 2017;74:383–91.

[29] Guo W, Yang Y, Liu C, Bu W, Guo F, Li J, Wang E, Peng Z, Mai H, You H. 3D printed TPMS structural PLA/GO scaffold: process parameter optimization, porous structure, mechanical and biological properties. J Mech Behav Biomed Mater 2023;142:105848.

[30] Zeng S, Ye J, Cui Z, Si J, Wang Q, Wang X, Peng K, Chen W. Surface biofunctionalization of three-dimensional porous poly (lactic acid) scaffold using chitosan/OGP coating for bone tissue engineering. Mater. Sci. Eng.: C 2017;77:92–101.

[31] Ma Z, Mao Z, Gao C. Surface modification and property analysis of biomedical polymers used for tissue engineering. Colloids and Surfaces B: Biointerfaces 2007;60(2):137–57.

[32] Alksne M, Kalvaityte M, Simoliunas E, Rinkunaite I, Gendviliene I, Locs J, Rutkunas V, Bukelskiene V. In vitro comparison of 3D printed polylactic acid/hydroxyapatite and polylactic acid/bioglass composite scaffolds: insights into materials for bone regeneration. J Mech Behav Biomed Mater 2020;104:103641.

[33] Islam MS, Abdulla-Al-Mamun M, Khan A, Todo M. Excellency of hydroxyapatite composite scaffolds for bone tissue engineering. Biomaterials 2020;10:1–22.

[34] Jarcho M. Calcium phosphate ceramics as hard tissue prosthetics. Clin. Orthop. Relat. Res.® 1981;157:259–78.
[35] Ratnayake JT, Mucalo M, Dias GJ. Substituted hydroxyapatites for bone regeneration: a review of current trends. J. Biomed. Mater. Res. Part B: Applied Biomater. 2017;105(5):1285–99.
[36] Ishaug SL, Yaszemski MJ, Bizios R, Mikos AG. Osteoblast function on synthetic biodegradable polymers. J. Biomed. Mater. Res. 1994;28(12):1445–53.
[37] Athanasiou KA, Agrawal CM, Barber FA, Burkhart SS. Orthopaedic applications for PLA-PGA biodegradable polymers. Arthroscopy: The J. Arthros. Related Surgery 1998;14(7):726–37.
[38] Tanodekaew S, Channasanon S, Kaewkong P, Uppanan P. PLA-HA scaffolds: preparation and bioactivity. Procedia Eng 2013;59:144–9.
[39] Kang HG, Kim SY, Lee YM. Novel porous gelatin scaffolds by overrun/particle leaching process for tissue engineering applications. J Biomed Mater Res B Appl Biomater 2006;79(2):388–97.
[40] Roether JA, Boccaccini AR, Hench LL, Maquet V, Gautier S, Jérȷme R. Development and in vitro characterisation of novel bioresorbable and bioactive composite materials based on polylactide foams and Bioglass for tissue engineering applications. Biomaterials 2002;23(18):3871–8.
[41] Verheyen C, De Wijn J, Van Blitterswijk C, De Groot K, Rozing P. Hydroxylapatite/poly (l-lactide) composites: an animal study on push-out strengths and interface histology. J. Biomed. Mater. Res. 1993;27(4):433–44.
[42] Gutiérrez Sánchez M, Escobar Barrios VA, Guillén AP, Escobar-García DM. Influence of RGD peptide on morphology and biocompatibility of 3D scaffolds based on PLA/hydroxyapatite. ChemistrySelect 2019;4(43):12656–61.
[43] Akindoyo JO, Beg MD, Ghazali S, Alam A, Heim HP, Feldmann M. Synergized poly (lactic acid)–hydroxyapatite composites: biocompatibility study. J Appl Polym Sci 2019;136(15):47400.
[44] Akindoyo JO, Beg MD, Ghazali S, Heim HP, Feldmann M. Impact modified PLA-hydroxyapatite composites–Thermo-mechanical properties. Composites Part A: Appl. Sci. Manuf. 2018;107:326–33.
[45] Omigbodun FT, Oladapo BI, Osa-uwagboe N. Exploring the frontier of Polylactic Acid/hydroxyapatite composites in bone regeneration and their revolutionary biomedical applications–A review. J. Reinf. Plastics Comp. 2024 07316844241278045.
[46] Rodrigues N, Benning M, Ferreira AM, Dixon L, Dalgarno K. Manufacture and characterisation of porous PLA scaffolds. Procedia Cirp 2016;49:33–8.
[47] Temple JP, Hutton DL, Hung BP, Huri PY, Cook CA, Kondragunta R, Jia X, Grayson WL. Engineering anatomically shaped vascularized bone grafts with hASCs and 3D-printed PCL scaffolds. J. biomed. mater. res. Part A 2014;102(12):4317–25.
[48] Guo F, Wang E, Yang Y, Mao Y, Liu C, Bu W, Li P, Zhao L, Jin Q, Liu B. A natural biomineral for enhancing the biomineralization and cell response of 3D printed polylactic acid bone scaffolds. Int. J. Biol. Macromol. 2023;242:124728.
[49] Rana H, Chavada D, Thakkar V. Amalgamation of nano and 3-D printing technology: design, optimization, and assessment. Annals of 3D Printed Med. 2024;13:100144.
[50] Hodaei M, Maghoul P, Popplewell N. An overview of the acoustic studies of bone-like porous materials, and the effect of transverse acoustic waves. Int J Eng Sci 2020;147:103189.
[51] Huo Y, Lu Y, Meng L, Wu J, Gong T, Zou Ja, Bosiakov S, Cheng L. A critical review on the design, manufacturing and assessment of the bone scaffold for large bone defects. Front Bioeng Biotechnol 2021;9:753715.
[52] Vazquez OR, Avila IO, Díaz JCS, Hernandez E. An overview of mechanical tests for polymeric biomaterial scaffolds used in tissue engineering. J. Res. Updates Polymer Sci. 2015;4(4):168–78.